Bioactive Catalytic Nanocompartments Integrated into Cell Physiology and their Amplification of a Native Signalling Cascade

Andrea Belluati[a], *Ioana Craciun*[a], *Cornelia G. Palivan*[a,]*

Department of Chemistry, University of Basel, Mattenstrasse 24a, BPR 1096, 4058 Basel, Switzerland

ABSTRACT

Bioactive nanomaterials have the potential to overcome the limitations of classical pharmacological approaches by taking advantage of native pathways to influence cell behavior, interacting with them and eliciting responses. Herein, we propose a cascade system mediated by two catalytic nanocompartments (CNC) with biological activity. Activated by nitric oxide (NO) produced by inducible nitric oxidase synthase (iNOS), soluble guanylyl cyclase (sGC) produces cyclic guanosine monophosphate (cGMP), a second messenger that modulates a broad range of physiological functions. As alterations in cGMP signaling are implicated in a multitude of pathologies, its signaling cascade represents a viable target for therapeutic intervention. Following along this line, we encapsulated iNOS and sGC in two separate polymeric compartments that function in unison to produce NO and cGMP. Their action was tested *in vitro* by monitoring the

derived changes in cytoplasmic calcium concentrations of HeLa and differentiated C2C12 myocytes, where the produced second messenger influenced the cellular homeostasis.

KEYWORDS

catalytic nanocompartments, cyclic guanosine monophosphate, nitric oxide, smooth muscle, cascade reaction

The cascade reaction mediated by nitric oxide synthase (NOS) and guanylyl cyclase (GC) has wide-spanning effect and its fine-tuning is essential for cell signalling. The malfunction of one or both of the enzymes has a drastic effect on the homeostasis of living organisms but also influences the growth and differentiation behaviour of cells.[1, 2] Inducible, endothelial and neuronal NOS (iNOS, eNOS and nNOS, respectively) are a family of enzymes that oxidize L-arginine to L-citrulline, producing nitric oxide (NO), which readily diffuses through membranes and plays a role in smooth-muscle relaxation, regulation of apoptosis, ion channel activity, mitochondrial function and immune response.[3, 4] While the -calcium-independent- iNOS is usually not linked to receptor-dependent processes, it is still involved in inflammatory vasodilation and other non-toxigenic pathways.[5-7] Deficiencies in the nNOS and eNOS are linked to muscular dystrophy and nephropathy;[8, 9] while iNOS has recently been suggested to be involved in compensating eNOS malfunctioning, with cardioprotective effects.[10]

Guanylyl cyclases (GC), the signalling partners of NOS, are widely distributed signal-transduction enzymes. Binding of NO, produced by NOS, to the heme moiety of the soluble guanylyl cyclase (sGC) induces the transition to activated sGC, which can then quickly convert guanosine-5'-triphosphate (GTP) into the second messenger cyclic 3,5-guanosine monophosphate

(cGMP) and pyrophosphate (PPi). cGMP acts as a ubiquitous second messenger in a variety of processes, through intra- and intercellular signalling cascades, regulating the activity of a number of downstream proteins, including cGMP-dependent protein kinase G (PKG), cGMP-dependent phosphodiesterases and cyclic nucleotide-gated ion channels. These pathways are involved in smooth muscle relaxation and vasodilation or immunomodulation[11] in regulating cell growth initiation and differentiation[2], cholinergic neurotransmission[12] and well as in photo-transduction in the vertebrate retina.[13] Aberrant cGMP signaling as a result of mutations in sGC has been associated with a number of diseases, such as retinal dystrophies (Leber's`congenital amaurosis, dominant cone-rod dystrophy, cone dystrophy and central areolar choroidal dystrophy).[11]

Current pharmacological research aims to replace whole cellular pathways that are damaged or missing, and disciplines such as tissue engineering and synthetic biology often need metabolome-spanning agents. These extensive modifications are usually achieved *via* genetic engineering, but when the need for transient modifications of cell behavior arises (*e.g.* cell differentiation, gene induction) this could be obtained *via* the *in situ* production of natural messenger molecules with known physiological effects.

A possible tool in enzyme supplementation or even cell engineering that can be used to correct aberrant signaling pathways, is the use of specialized reactive compartments, as the spatiotemporal compartmentalization of reactions allows a more precise kinetic regulation,[14] creating specialized environments and protecting them from the exterior.[15] This concept has already been applied in nanotechnology where enzymes are entrapped into nano-sized objects such as protein cages, or lipid/polymer based compartments.[16, 17] Polymer compartments with nanometer sizes, called polymersomes are particularly appealing to host *in situ* enzymatic reactions, as their membrane is more stable than that of liposomes and can be functionalized with different moieties to support

targeting or immobilization on surfaces, while, if appropriately selected, retaining biocompatibility.[18-20] When loaded with enzymes and rendered permeable for substrates/products, polymersomes serve as efficient catalytic nanocompartments (CNCs) with a broad range of applications depending on the encapsulated enzyme.[19] To this day, CNCs have been used in biological settings as organelle models,[21-23] sensors, detoxifying agents,[24] to produce or to release/activate prodrugs,[19, 25] meaning their effect was parallel to the cell metabolism and had a limited influence on the cell itself.

Here, we present how such catalytic nanocompartments are combined to work in tandem and serve to support the iNOS-sGC enzymatic cascade by enhancing it in the cell pathway. We chose to encapsulate separately the enzymes to overcome the limitations due to coencapsulation, and to offer a modular system, as in some cases the enzymes of a cascade cannot be easily coencapsulated, if one is more sensitive, or has different size or surface charge than the other and therefore requires a different formulation procedure. We investigated these enzymes separately encapsulated into CNCs composed of a poly(dimethylsiloxane)-*block*-poly(2-methyl-2-oxazoline)-*block*-poly(dimethylsiloxane) (PMOXA-*b*-PDMS-*b*-PMOXA) membrane. The membrane of the CNCs was permeabilized by insertion of the bacterial Outer membrane protein F (OmpF) to allow the diffusion of substrates/products and thus promote the *in situ* enzymatic reaction. The role of the polymersomes was to protect the enzymes from the external environment and transport them to cells.[26, 27] We then characterized the assembled iNOS-CNCs and sGC-CNCs both physically (light scattering, electron microscopy, fluorescence microscopy, nanoparticle tracking analysis) and functionally (fluorometric assays). We studied their biological activity on HeLa and smooth muscle C2C12 cells, using the cytoplasmic concentration of calcium as a functionality parameter

to demonstrate whether the CNCs in tandem work in physiological conditions and elicit cellular responses.

As such cascade is already present in cells, our CNCs are able to act as a metabolism-enhancing cascade derived from nano-sized compartments, with possible applications as cell differentiation agents, for instance in regenerative medicine or cardiovascular therapies.[28-30] The advantage of our binary CNC system derives from their ability to induce changes in cell homeostasis without the addition of any other compound, only using the arginine and GTP naturally present in the cell or in the culture medium.[31-33] This allows acting on cell signaling pathways, effectively integrating their functionality into native cell metabolism and physiology, instead of operating orthogonally on cells, with no cell communication.

Results and discussion

Encapsulation of iNOS and sGC into individual CNCs

We encapsulated the two enzymes into biocompatible $PMOXA_6$-*b*-$PDMS_{44}$-*b*-$PMOXA_6$ polymeric assemblies *via* film rehydration.[34, 35] This technique consists of vacuum drying the block copolymer to obtain a film, then adding the rehydration buffer containing the molecules of interest. Continuous stirring promotes the swelling of the copolymer film leading to self-assembly and formation of nano-assemblies entrapping the solutes (Figure 1A).

The $PMOXA_6$-*b*-$PDMS_{44}$-*b*-$PMOXA_6$ block copolymer used in this study self-assembled into supramolecular assemblies with a radius of gyration R_g = 102 ± 16 nm and radius of hydration R_h = 103 ± 8, PDI 0.4. The R_h/R_g ratio (ρ-factor), being close to 1, meant that we obtained hollow spherical vesicles, *i.e.* polymersomes (Fig. 1B).[36] Upon permeabilization of the membrane with OmpF and encapsulation of iNOS, the radii and spherical morphology of the CNC did not change

(iNOS-CNC, R_g =102 ± 23 nm and R_h = 104 ± 9 nm, PDI 0.5 and ρ-factor 0.99 in both cases). Also, in the case of sGC-CNC upon permeabilization and enzyme encapsulation no changes in the compartments was observed (sGC-CNC, R_g = 104 ± 14 nm and R_h = 101 ± 6 nm, ρ-factor 1.03), indicating the polymeric vesicular structures are unaffected by the presence of proteins either in the lumen or within the membrane.

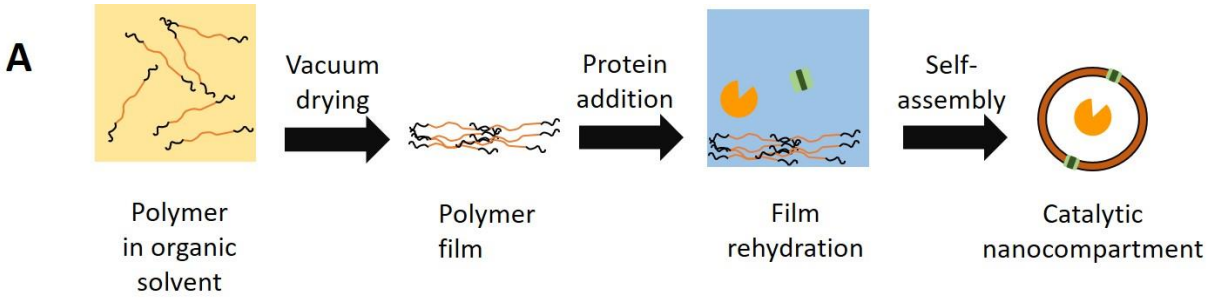

B

	R_g (nm)	R_h (nm)	ρ (R_g/R_h)	Concentration (vesicles ml^{-1})
No protein	102 ± 16	103 ± 8	0.99	$1.4 \times 10^{12} \pm 0.1 \times 10^{12}$
iNOS (+OmpF)	102 ± 23	104 ± 9	0.99	$1.7 \times 10^{12} \pm 0.5 \times 10^{12}$
sGC (+OmpF)	104 ± 14	101 ± 6	1.03	$1.8 \times 10^{12} \pm 0.1 \times 10^{12}$

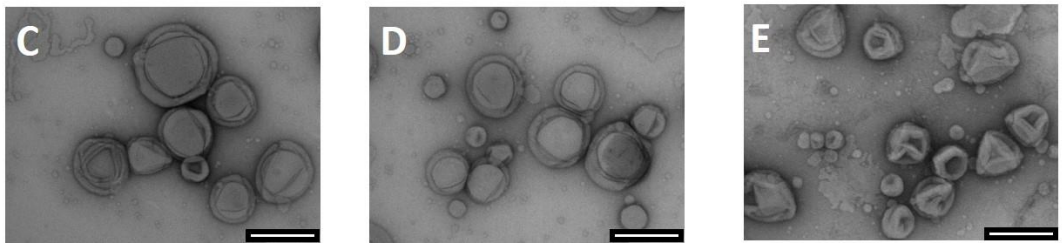

Figure 1. A: fabrication workflow of the CNCs. B: table of Rg, Rh and vesicle concentration for the CNCs with and without proteins (enzymes and OmpF). C: TEM micrograph of empty polymersomes. D: TEM micrograph of iNOS-CNC E: TEM micrograph of sGC-CNC. Scale bar for TEM micrographs: 200 nm.

For an efficient CNC cascade reaction, and its administration to living tissues, it is imperative to have a balance between the amounts of each compartment. Using nanoparticle tracking analysis (NTA) we ensured that there was no significant difference in polymersome concentration between the two CNCs. Polymersomes had concentrations between $1.4\times10^{12}\pm 0.1 \times 10^{12}$ and $1.8\times10^{12} \pm 0.1 \times 10^{12}$ vesicles mL^{-1} (Figure 1B). Using this method, we also reconfirmed the radii, with R_h of 96 ± 19 nm for empty polymersomes, 95± 19 nm for iNOS-CNC and 96 ± 17 nm for sGC-CNC (Fig. S1). The morphology of iNOS or sGC containing nanoassemblies was observed by TEM, showing spherical shapes with the deflated membrane typical of polymersomes under vacuum (Figure 1C-E); the micrographs also show the common size dispersity of polymersomes. [18-20]

Having determined the concentration of each CNC, next we calculated the encapsulation efficiency as the amount of enzyme encapsulated per compartment. To achieve this, we fluorescently labelled each enzyme. iNOS was labelled with an average of 1 ± 0.3 ATTO488 dye molecules per enzyme while sGC was labelled with an average of 2 ± 0.9 DyLight633 dye molecules per enzyme. Having successfully labelled the enzymes we proceeded to measure fluorescence correlation spectroscopy (FCS) of labelled enzymes and enzyme-loaded vesicles. This technique allows us both to use very low concentrations of the fluorescently labelled enzymes, and to measure differences in diffusion times of fluorescent molecules to correlate it to the hydrodynamic radius of the molecule/supramolecular assembly. The shift to the right of the autocorrelation curves is evidence of an increase of diffusion time (Figure S2A-B), respectively from the free dye to the dye-labelled enzyme and enzyme-loaded CNC. From the measured diffusion times of enzyme loaded CNC, we confirmed the order of magnitude of the hydrodynamic radii, R_h of 94± 56 nm for iNOS-CNCs and 85± 33 nm for sGC-CNCs. Similar R_h were also found

by fluorescently staining the polymersomes' membrane with the hydrophobic BODIPY 630/650 (115 ± 27 nm and 96 ± 37 nm, respectively), indicating again a similar size of both CNCs, within the standard deviation.

Finally, brightness measurements, serving to compare the brightness of poplymersomes and enzymes, allowed us to determined that iNOS CNCs contained 5 ± 4 enzymes per compartment and sGC-CNC contained 3 ± 1 enzymes per compartment. Using a 2-component model, discriminating between enzyme and vesicle signal, we observed that 1% of iNOS was still free in solution after purification, and less than 0.1% of sGC was free in solution following purification, probably due to low unspecific adsorption on the membrane. The encapsulation efficiency, measured by recovering the un-encapsulated enzyme fraction by SEC, was 13% ± 3% for iNOS and 89%± 1% for sGC (n = 3).

By performing a complete physico-chemical analysis of the CNCs, we established that spherical, hollow structures are formed and are not influenced by the presence of enzymes in the rehydration buffer, or OmpF, which was demonstrated to insert only into the polymer membrane,[37] resulting in CNCs with comparable polymersome concentrations, vesicle radii and amount of encapsulated enzyme.

CNC kinetics

The cascade reaction between iNOS and sCG free in solution was first tested using the GTP analog mant-GTP that is transformed by sGC upon NO production into the fluorescent mant-cGMP final cascade product. The reaction proceeded with high speed, which ended in a plateau after 2 minutes (Figure S3), as expected from the high turnover rate of both iNOS and sGC,[38, 39] thus showing that we could follow both reactions by measuring the final product mant-cGMP. On contrary, when either NADPH or arginine (on which iNOS depends) were not included in the

cascade reaction, the fluorescence associated with the mant-cGMP final cascade product was significantly lower. The low fluorescence observed in absence of NADPH might be due to residual cofactor co-purified with the enzyme, but was negligible, compared to the full cascade.

The first enzyme of the cascade, iNOS, was then encapsulated inside polymersomes equipped with OmpF (iNOS-CNC), and its activity compared to iNOS free in solution was determined by monitoring the fluorogenic reaction between NO, as product of the enzymatic reaction, and DAF (Figure 2), whereas no activity was detected without OmpF. The ratio between the CNC activity and free enzyme activity was calculated to be 112 ± 47%. A CNC activity equal or higher to that of the free enzyme is not surprising, as it was already shown that encapsulated enzymes could theoretically reach the same or higher activity than when free in solution thanks to the confinement effect, provided that the diffusion of substrates is not a limiting factor. [26] In this respect, we can conclude that the diffusion of arginine across OmpF is very fast,[40] and that Vmax is likely decreased to a lesser degree than previously observed for other reactions.[26] As a control, CNC without OmpF showed no activity.

We then further focused on the encapsulated cascade, to progress with the mimicking of natural pathways. When both iNOS and sGC are encapsulated within their respective CNCs, the overall cascade reaction exhibits a significant decrease, compared to the enzymes free in solution (Figure 4). In the timeframe of the cascade in bulk, after 10 minutes no activity is detected. Only after at least 4 hours, we begin to see an appreciable conversion of mant-GTP to mant-cGMP, continuing steadily for 12 hours, eventually reaching 49 ± 19 % of the maximal value obtained with the free enzymes. This decrease in activity is due to the diffusion of substrates across OmpF, which, as demonstrated in Figure 3, does not affect iNOS-CNC, nor is it dependet on nitric oxide, a small and fast diffusing molecule that is not hindered by the CNCs' membrane. The main limiting factor

must be ascribed to the diffusion of the sGC substrates. The devised assay is based on the GTP-derivative mant-GTP (656 Da), whose molecular weight is around the cut-off of OmpF,[41] strengthening the evidence that its bulkiness is the main limiting factor in the overall activity of the CNCs in the cascade (Figure 4). Such behavior reveals a complex mechanism, where overall cascade kinetics find a bottleneck in the diffusion of the substrate. To confirm that the limitation was caused by the diffusion across the membrane of the modified GTP, we co-encapsulated mant-GTP together with inactive sGC (before the presence of NO produced by the iNOS-CNC upstream), this time retained inside the cavity of polymersomes thanks to its extremely slow diffusion across OmpF to the bulk. Doing so yielded a 99 ± 9 % retained enzymatic activity as compared to the enzymes free in solution, over the course of 12 hours, but with a completely different kinetic: we observe a fast reaction rate in the first few minutes, which plateaus after 2 hours. At the 4 hours' mark, having consumed the co-encapsulated substrate, the enzyme starts to rely on the external mant-GTP now diffusing in, as seen in the previous scenario. The diffusion across the CNC membrane is thus a major limiting step for a cascade between CNCs when substrates have molecular weight close to the cut-off of the porin, as already reported for other cascades between CNCs equipped with OmpF.[26] We can also exclude that the higher starting signal for co-encapsulated mant-GTP is due to its higher concentration, as no signal was detected in the control samples composed of the same system but without the necessary components to allow the reaction to proceed (Figure S4).

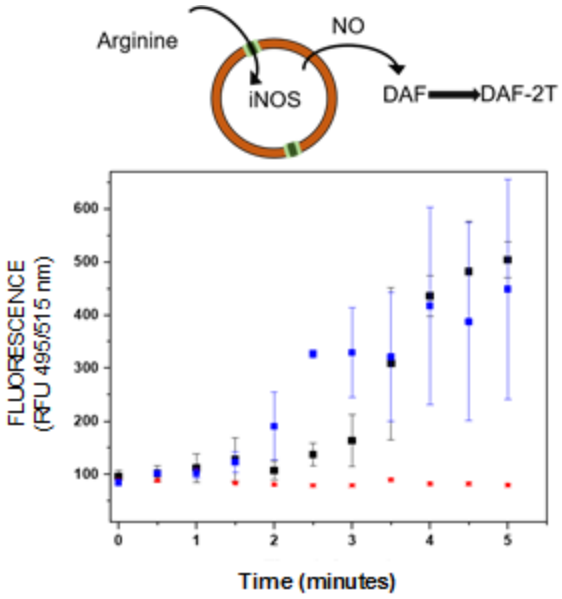

Figure 2. Reaction scheme and activity (relative fluorescence units, RFU) of free iNOS (black) iNOS-CNC (blue) and iNOS-CNC without OmpF (red), showing the similar values for both encapsulated and unencapsulated enzymes. Values given as mean ± SD, n=3.

Despite the limitations provided by the interplay between intrinsic CNC features (diffusion across OmpF) and assay-dependent limitations (the substrate's size), we showed that the compartments worked in tandem, and successfully provided the final product cGMP with a slow and constant flow over a long period, akin to the controlled release of drugs. This was obtained through a careful selection of parameters: sGC is a NO-dependent enzyme, but excessive NO also deactivates the enzyme, [42, 43] which is also competitively inhibited by its product;[44]higher concentrations of iNOS-CNCs lead to a very complex fluorescence profile (Figure S5A), as did higher concentrations of co-encapsulated mant-GTP (Figure S5B). This was likely caused by, respectively, an excess of nitric oxide, inactivating the enzyme for some seconds at time, or the product mant-cGMP, which inhibits the enzyme, compounded by the possible self-quenching of

high concentrations of mant-cGMP, slowly diffusing out. This led to a high heterogeneity of kinetic profiles, with fluorescence peaks and minimums.

An additional benefit of encapsulation inside CNCs is enzyme resilience: when both free iNOS and sGC were subjected to the same workup and storage conditions as encapsulated enzymes, they lost activity (Figure S6A), while the encapsulated ones were still functional. Enzymes non-specifically adsorbed to the vesicles' outer membrane were also intrinsically unstable and had no catalytic activity (Figure S6B) after workup and storage at 4 °C. Overall, such findings suggest that any unencapsulated enzyme remaining after the purification would retain no activity by the assay's time.

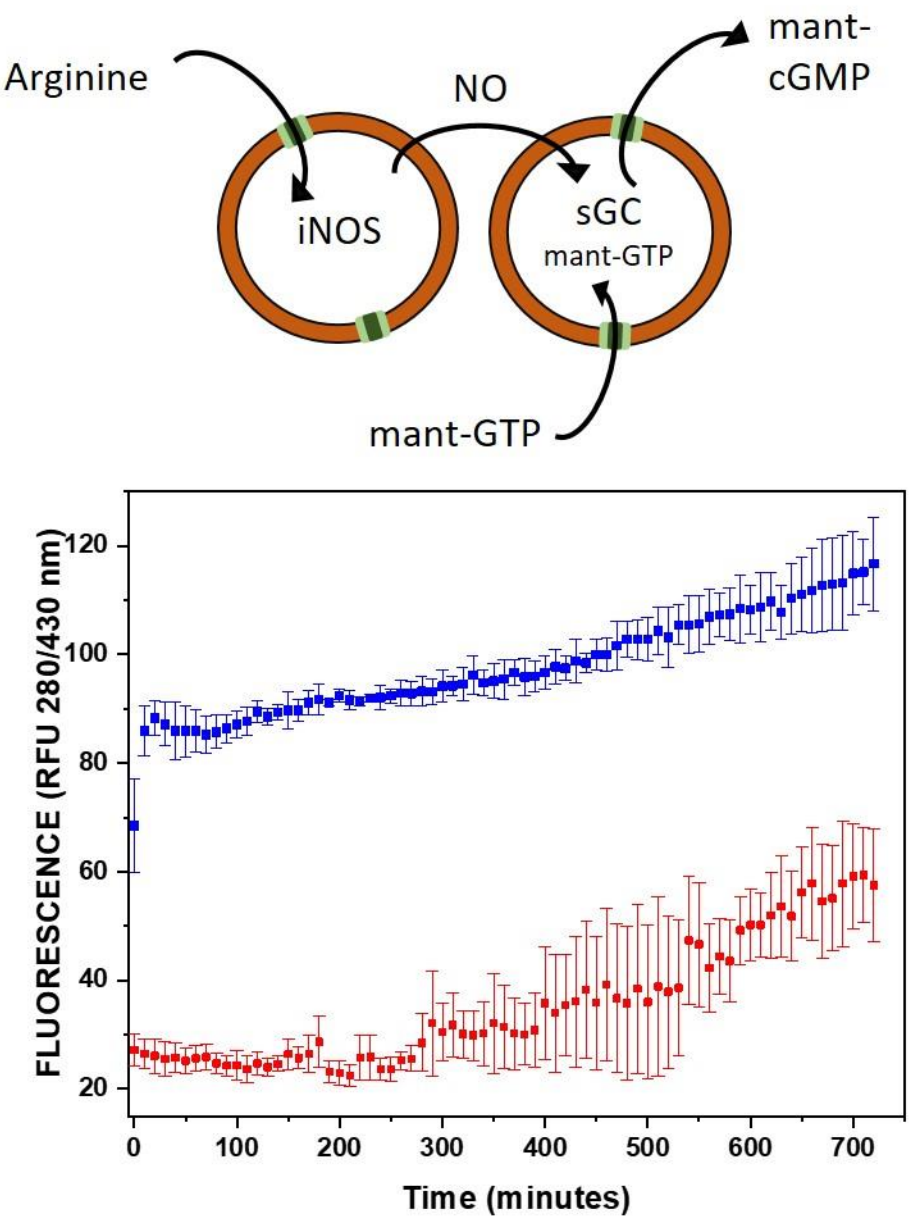

Figure 3. Scheme and activity (relative fluorescence units, RFU) of the cascade mediated by iNOS-CNC with: sGC-CNC (red) and mant-GTP co-encapsulated with sGC (blue). Values given as mean ± SD, n=3.

CNC kinetics interact with cells and influence their homeostasis

As CNCs have been used in biological settings as sensors, detoxifying agents, to produce or to release/activate prodrugs,[19] they did not participate to the cell metabolism, with only one example aimed at complementing defective pathways.[45] Having shown that a cascade reaction successfully produces cGMP as a second messenger, we set to study the interaction of our CNCs with live cells, using only the naturally present arginine and GTP substrates and without using mant-GTP, thus overcoming its bulkiness.[31-33] In nature, the NO/cGMP signalling cascade acts on calcium channels resulting in an increase in free cytoplasmic calcium along with other downstream cellular effects. To determine if our CNCs integrate and function within the cellular metabolism either through extracellular or intracellular signaling, we chose to follow cytoplasmic calcium levels of cells exposed to the CNCs, *i.e.* the amplification of a native pathway. This was accomplished by monitoring the fluorescence of the calcium-sensitive and cell-permeant Fluo-4-AM dye, added separately from the CNCs, by live cell imaging, and compared to the baseline level of untreated cells. Fluo-4-AM is uptaken by the cell and metabolized by esterases so that it is retained for a longer time, and increases its brightness when complexing calcium. $PMOXA_6$-*b*-$PDMS_{44}$-*b*-$PMOXA_6$, like other PMOXA-*b*-PDMS-*b*-PMOXA polymers, was shown to be non-toxic and polymersomes are unspecifically uptaken by cells over the course of hours.[26, 27, 46] With a cascade that does not require the addition of substrates, but can find them in the culture medium or within the cell, our tandem of CNCs are expected to exert their activity as soon as they administered. For this reason, we analyzed two scenarios: the short-term effect of CNCs added to cells and the long-term effect after they are uptaken. By incubating Atto488- iNOS labelled CNCs and DY633 sGC labelled CNCs together with HeLa cells, we could see that they become internalized starting at 12 hours after administration -most likely *via* micropinocytosis, due to their size, and localizing

mainly in the cytoplams[27, 47]- thus allowing to discriminate temporarily between extra- and intracellular action (Figure 5A, Figure S7 and Movie S1).

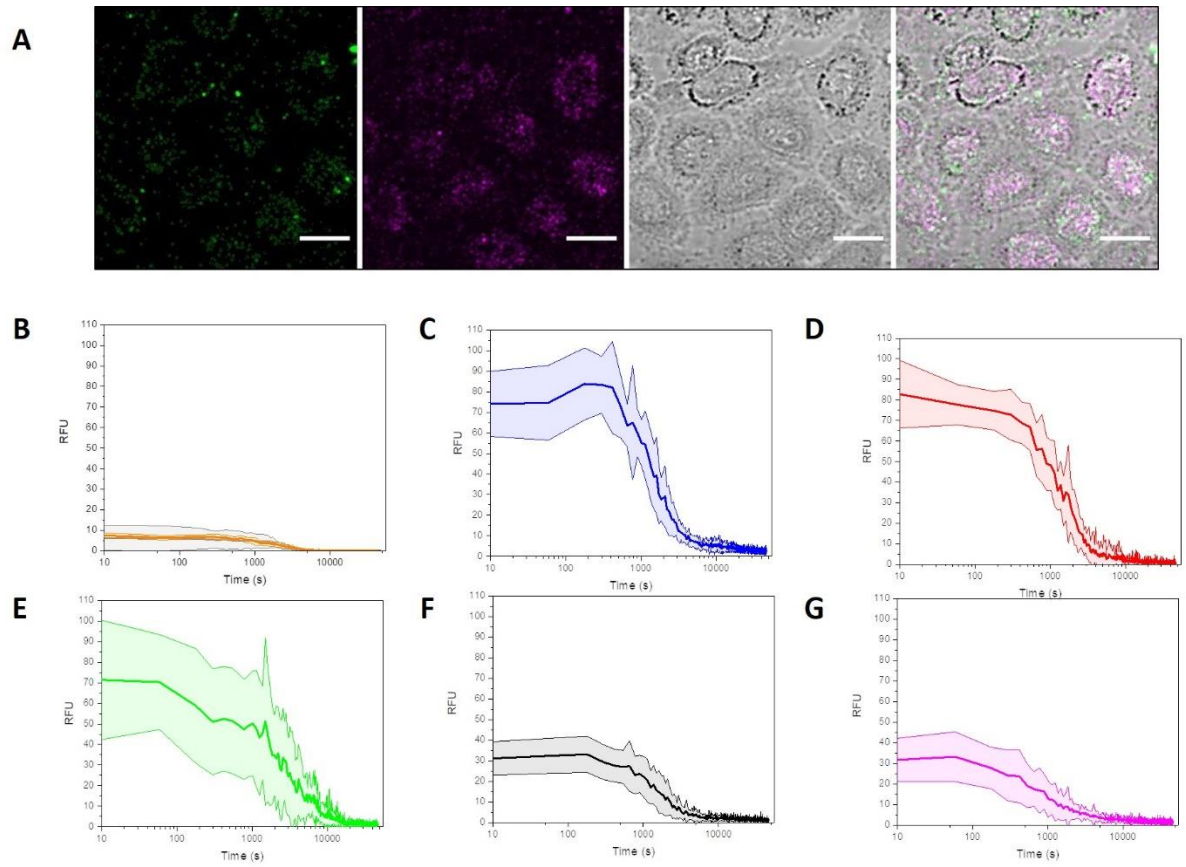

Figure 4. A: CLSM micrographs of iNOS-ATTO488-labeled CNCs (green), sGC-DY Light 633-labeled sGC CNCs (magenta), HeLa cells (brightfield) and overlay, after 14h of incubation. Scale bar: 10 µm. B: cytoplasmic [Ca^{2+}] of HeLa with no treatment (orange) and treated with empty polymersomes (grey). C: cytoplasmic [Ca^{2+}] of HeLa treated iNOS-CNC and sGC-CNC in cell medium. D: cytoplasmic [Ca^{2+}] of HeLa treated with NO-donor SNAP and cGMP. E: cytoplasmic [Ca^{2+}] of HeLa after the uptake of iNOS- and sGC-CNC. F: cytoplasmic [Ca^{2+}] of HeLa treated with iNOS-CNC only. G: cytoplasmic [Ca^{2+}] of HeLa treated with sGC-CNC only. Y-axis: arbitrary fluorescence units. Values given as mean ± SD, n=11.

Almost no fluorescence signal was detected for either untreated control cells or cells treated with control empty vesicles (Figure 5B).

When the CNCs (1 to 1 CNCs ratios) and Fluo 4-AM were added extracellularly to HeLa cell cultures and measured right after addition, there was a quick increase in fluorescence intensity (<5 minutes) within the cellular cytoplasm indicating that the cascade immediately induced the opening of calcium-specific channels, quickly increasing the cytoplasmic [Ca^{2+}] (Figure 4C, Movie S2). Since the CNCs, are added to the cell culture and monitoring of internal [Ca^{2+}] commences with only a 5-minute delay, the signaling cascade exerts its effect primarily extracellularly. The initial increase in [Ca^{2+}] was followed by a slow decrease (2.5 hours) in fluorescence back to resting levels, due to both the decrease in [Ca^{2+}] and eventual excretion of the dye *via* active transport channels.[48] As a positive control, we added to the cell culture both the NO-donor SNAP and cGMP, *i.e.* directly the products of the enzymatic cascade reaction, at similar concentrations as would be produced by the CNCs. We observed a similar increase in cytoplasmic [Ca^{2+}] as when the CNCs were added (Figure 4D), confirming that the increase in [Ca^{2+}] observed after addition of the CNCs is a direct result of NO/cGMP production.

To study the intracellular effect of the CNCs on [Ca^{2+}], we incubated the cells in presence of the CNCs for 24 h, followed by rigorous washing of the cells to remove non-uptaken CNCs and loading of the cells with the calcium sensitive Fluo-4-AM dye, ensuring that the effect would only come from internalized CNC and not from non-uptaken CNCs. Thanks to the slow and constant activity of sGC-CNCs, fuelled by iNOS-CNC, even internalized CNCs continued to produce cGMP modulating cytoplasmic [Ca^{2+}] (Figure 4E). In fact, they show a very similar fluorescence

profile when fresh medium and Fluo-4-AM were subsequently added, after a prior 24h incubation with the CNCs. The similar values obtained for internalized CNCs as for cells measured in presence of externally located CNCs, reveal that they retain their activity for a long time inside the cells, with long-term effects comparable to that of a single exposure.

The addition of only iNOS- or sGC-CNCs showed a much lower activity, suggesting that only one kind of CNC is not enough to increase the calcium-derived fluorescence above a baseline signal (Figure 4F and 4G respectively). A slight increase in fluorescence is indeed observed due to interactions between the iNOS-CNC and native sGC or the sGC-CNC with trace endogenous NO; however, to obtain a complete and effective signalling cascade, both CNCs are required to ensure the quick production of NO and the action on its receptor sGC to cause a drastic change in cytoplasmic [Ca^{2+}] levels.

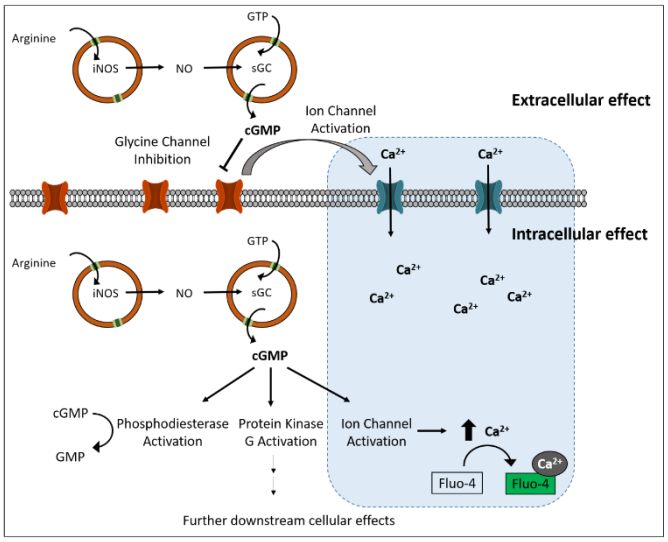

Figure 5. Mechanism of cell-CNC interaction and possible affected pathways in cells: the CNCs exert their action both extra- and intracellularly, and this can be monitored using the cytoplasmic [Ca^{2+}] as biomarker.

To compare the rate of change in cytoplasmic [Ca^{2+}] we first normalized the mean fluorescence profiles, thus disregarding the differences in initial [Ca^{2+}], and setting the profile of non-treated cells as the reference over time decrease. It is apparent that SNAP+cGMP treated cells follow a very similar kinetic to that of untreated cells, indicating that cytoplasmic [Ca^{2+}] levels return quickly back to base levels. Uptaken iNOS-CNC+sGC-CNC show an initial rate close to the reference, which then slows down after 3-4h (Figure S8A-B). This second, slower rate of decrease could be due to further downstream intracellular signalling pathways that increase cytoplasmic [Ca^{2+}] with a delay and that cannot be accessed when the CNCs are extracellular. Interestingly, external iNOS-CNC+sGC-CNC and iNOS-CNC treated cells maintain a constant [Ca^{2+}] for 3 hours, then dropping with a similar rate as the reference cells. External sGC-CNC induce a slower rate of Ca^{2+} release than the reference, likely due to the slow production of cGMP. Such behavior shows clearly that the localization of the CNCs has different effects on the cell physiology, and that they can perform their function at least for 24h after being administered, a favorable characteristic for long-lasting applications.

The immediate effect observed on cells measured 5 minutes post CNC addition (Figure 4B and 4C) cannot derive from the canonical, well-known effect of cGMP on cGMP-dependent PKG and cGMP-gated ion channels,[49] as those are intracellular pathways. Rather, this must come from the effect of extracellular cGMP on glycine ion channels, inducing activation of calcium ion channels,[50, 51] along with the diffusion of NO to cells (which, on the other hand, involves the canonical pathways mentioned before). This is also in line with the fact that HeLa cells usually express a low amount of PKG.[52] On the other hand, the detected intracellular activity should not be due to non-internalized CNCs (as they are removed by washing), but rather to cAMP-activated Ca^{2+} influx, as cyclic nucleotides cGMP and cAMP are known to crosstalk and interact with non-

specific targets and, as mentioned, PKG is generally underexpressed in HeLa.[49, 53] Overall, these findings suggest that the CNCs not only affect cytoplasmic calcium levels, but also have different protein targets on the cell surface and further downstream proteins within the cytoplasm, resulting in different calcium release rates, depending on the CNC localization (Figure 5).

Next we analysed the effect of the CNCs on cytoplasmic [Ca^{2+}] in differentiated C2C12 myocytes, which are more sensitive to calcium levels.[54]

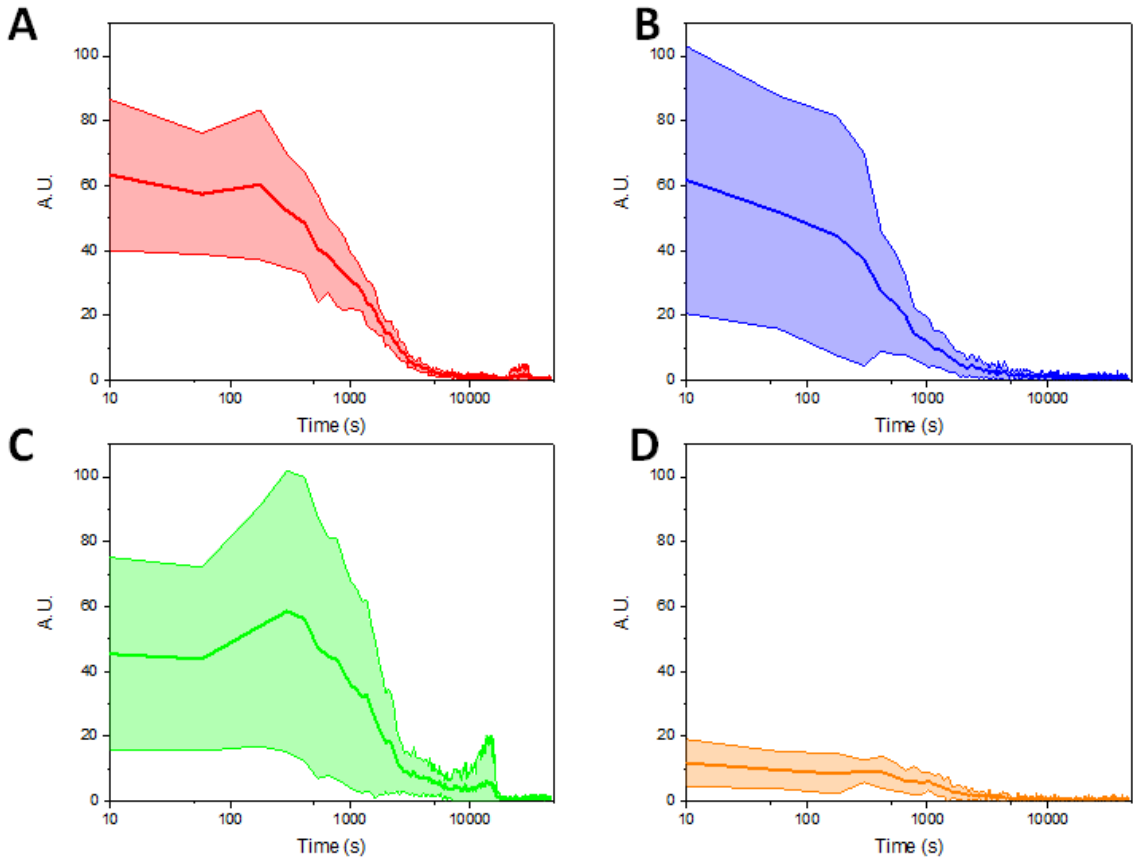

Figure 6. A: cytoplasmic [Ca^{2+}] of C2C12 treated with NO-donor SNAP and cGMP. B: cytoplasmic [Ca^{2+}] of C2C12 treated iNOS-CNC and sGC-CNC in cell medium. C: cytoplasmic

[Ca^{2+}] of HeLa after the uptake of iNOS- and sGC-CNC. D: cytoplasmic [Ca^{2+}] of C2C12 with no treatment. Y-axis: arbitrary fluorescence units. Values given as mean ± SD, n=11.

In muscle cells, the NO/cGMP signalling cascade results in a complex modulatory effect of [Ca^{2+}], where an increase due to release of stored calcium is first observed followed by a slow depletion.[55, 56] For the positive control, where the NO-donor SNAP and cGMP were used, a high cytoplasmic [Ca^{2+}] was measured (Figure 6A). The CNCs, both freshly added to the medium (Figure 6B) and after a 12 hours incubation and subsequent uptake (Figure 6C) showed high initial cytoplasmic [Ca^{2+}] values, marked by higher cellular variability (resulting in greater standard deviation).[57] Furthermore, the fluorescence signal, resulting from Fluo-4AM complexing cytoplasmic [Ca^{2+}], returned back to baseline levels in a shorter time frame as compared to HeLa cells, indicating a calcium depletion event. Added to the lower resilience of C2C12 cells, with some apoptosis events during imaging, it all hints to the higher susceptibility to calcium levels and derived stress (Movie S3). Such susceptibility plays a role in muscle dystrophy and atrophy.[58, 59] For the negative, no treatment-control, again only a background fluorescence was observed (Figure 6D).

Muscle cells are thus more susceptible to the CNC cascade, as cGMP finds more targets, not only in the cell membrane or in the cytoplasm, but also regulates the release of calcium from the sarcoplasmic reticulum.[55]

Conclusions

Enzymatic cascades between different catalytic nanocompartments present both the challenge of communication between compartments and the advantage of increased enzyme stability and modularity. Such potential has only been partially investigated, with very few studies using catalytic nanocompartments as bioactive constructs. In this work, we present a two-compartment

system where iNOS and sGC operate in unison as in a native cascade. We encapsulated them in PMOXA-*b*-PDMS-*b*-PMOXA polymersomes and characterized the derived CNCs both physically and functionally. We then integrated them in the metabolism of cells and studied their *in vitro* activity, as this cascade successfully used natively present substrates to produce an important bioactive compound, cGMP. The effect of cGMP production was monitored by measuring cytoplasmic calcium levels over time, showing that the concerted action of both iNOS-CNC and sGC-CNC was needed to elicit the highest response (inducing calcium influx). These findings demonstrate that CNCs can be directly integrated and act on cell physiology, using the substrates already present in the extracellular medium. Additionally, the production of both NO and cGMP will allow the design of more complex nanoassemblies with the potential to induce wide range cell changes, functioning as signalling agents for applications that range from pharmacology to tissue engineering and synthetic biology. Further research will have to elucidate the dose-response behaviour to CNCs and confirm the molecular mechanisms of CNC-cell interaction.

Experimental

Chemicals

, Outer membrane porin F (OmpF) was obtained according to previously published procedure.[26]

Soluble guanylyl cyclase (bovine) was purchased from SantaCruz Biotechnology (USA); DyLight 633 NHS ester and Fetal calf serum (FCS) were purchased from ThermoFisher Scientific (USA); mant-GTP (2'-(or-3')-*O*-(*N*-Methylanthraniloyl) Guanosine 5'-Triphosphate, Trisodium Salt) was purchased from Jena Bioscience (Germany); Nitric Oxide Cofactors (NOC) mix containing flavin adenine dinucleotide (FAD), flavin mononucleotide (FMN), and calmodulin was purchased from Oxford Biomedical Research (USA). FluoroBrite Dulbecco's Modified Eagle

Medium (DMEM) live cell imaging medium was from Gibco Life Sciences (USA). All other compounds were purchased from Sigma-Aldrich.

Copolymer used for polymersomes and CNS formation

The synthesis and the characterization (GPC, ^{1}H-NMR) of the amphiphilic block copolymer $PDMS_6$-b-$PMOXA_{44}$-b-$PDMS_6$ (M_w/M_n =1.6) have been performed according to reference[60].**Preparation of CNCs/polymersomes**

iNOS and GC catalytic compartments were obtained by the film rehydration method.**[61]** Briefly, 1 mL of a 4 mg mL^{-1} solution of $PMOXA_6$-*b*-$PDMS_{44}$-*b*-$PMOXA_6$ in ethanol was slowly evaporated in a rotary vacuum evaporator at reduced pressure until a film on the flask wall was formed. The polymer film was rehydrated overnight, at 4 °C, under continuous magnetic stirring with 1 ml of a solution of 1 mg mL^{-1} iNOS or 5 µg mL^{-1} sGC in PBS, to which either OmpF to a final concentration of 80 µg mL^{-1} or an equivalent volume of dialyzed octyl-glucopyranoside was added as a control.[26] iNOS solutions were supplemented with 40 µg mL^{-1} of NOC and nicotinamide adenine dinucleotide phosphate (NADPH) to a final concentration of 100 µM mL^{-1}, to contrast the slow diffusion of cofactors and NADPH across OmpF by co-encapsulating them with iNOS.[26, 41] In one case, mant-GTP was co-encapsulated with sGC (final concentration: 100 µM). After rehydration, the solutions were extruded 11 times through 200 nm track edge polycarbonate Whatman filters (Sigma Aldrich) at RT. The resulting CNCs were purified *via* size exclusion chromatography (SEC) on a 20 cm Sepharose 4B column, at RT. The unencapsulated iNOS (from OmpF-free and calmodulin-free sample) was recovered for quantification. Polymersomes self-assembled in similar conditions by rehydration with PBS only, served as control compartments.

Aliquots of the free enzymes were subjected to the same workup as the polymersomes/CNCs (same temperatures, extrusion, SEC), but either without encapsulation or added to preformed empty polymersomes and then re-purified, to test the stability of non-encapsulated enzymes at higher temperatures.

Fluorescent dye- labelling of iNOS and sGC

Stock solutions of iNOS (5 mg mL^{-1}) and GC (5 µg mL^{-1}) were prepared in 0.1M Na_2CO_3 buffer, pH 8.3. 5µL of a 1.5 mM Atto-488 NHS ester in DMSO solution was added to 1 ml of the iNOS stock solution and 5µL of 1.5 mM DyLight 633-NHS ester in DMSO was added to 1 ml of sGC solution. Both labelling reactions were mixed overnight at 4 ºC. Free dye was removed by dialysis (Spectrapore dialysis tube, MWCO 12kDA, Spectrum Laboratories Inc) against PBS at 4 ºC for 3 days with frequent buffer exchanges. Upon purification, labelled enzymes were used directly and polymersomes were formed as previously described. Labelled sGC was recovered from an OmpF-free sample (to avoid any residual signal) and used for quantification of encapsulated protein (see below).

Static and dynamic light scattering

Dynamic and static light scattering (DLS, SLS) were used to determine the size of the extruded polymersomes. SLS and DLS experiments were performed on a setup from LS instruments (Switzerland), equipped with a He-Ne 21 mW laser (λ = 632.8 nm) at scattering angles from 30° to 55° at 25 °C. The radius of gyration (R_g) was obtained from the SLS data fitted with a Guinier plot. The intensity versus angle curve of a diluted sample (to supress multiple scattering) was fit with a linear regression and the slope of the curve *m* was used to calculate R_g according to the equation

$$R_g = 10^9 \times \sqrt{3m}$$

Equation 1

In the case of DLS, second order cumulant analysis of the data between 30° and 155° was performed to obtain the hydrodynamic radius (R_h). The error is based on the error of the slope (%).

Nanoparticle tracking analysis (NTA)

NTA was used as further analysis of particle size and concentration, on a NanoSight NS300 (Malvern Panalytical Ltd., UK), using a flow cell (100 µL min^{-1}), 1:1000 concentration in freshly filtered PBS, yielding particle R_h and concentration (particle mL^{-1}).

Transmission electron microscopy (TEM)

CNC suspensions in PBS at 0.25 mg mL^{-1} were deposited on glow-discharged carbon grids (Quantifoil, Germany) stained with 1.5% uranyl acetate solution and deposited on carbon-coated copper grids. A transmission electron microscope (Philips Morgagni 268D) at 293 K was used.

Fluorescence correlation spectroscopy (FCS)

Polymersomes containing encapsulated iNOS-ATTO 488 or sGC-DyLight 633 were labelled with 100 nM BODIPY 630/650 (Thermo Fisher Scientific). All measurements were carried out using an LSM 880 confocal laser microscope (Carl Zeiss, Germany) with a 40x, 1.2 water immersion C-Apochromat objective lens. Measurements were performed at room temperature using a sample volume of 30 µL on a 22x50 mm glass slide. A 488nm argon laser was used to excite ATTO 488 and a 633 nm HeNe laser was used for DyLight633 and BODIPY 630/650. The two lasers were passed through MBS488 and MBS488/561/633 filters and the signals were detected in the range of 500-532 nm and 657-690 nm, respectively. The pinholes were adjusted to maximize the count rate using the respective free dye in PBS and the sample volumes were 20 µL. Fluorescent fluctuations over time were recorded for 20 x 5 s. The raw data was processed and

analyzed using Zeiss software. Autocorrelation curves were fitted by a two-component model (except for dye-only samples).

$$G(\tau) = 1 + \left(1 + \frac{T}{1-T} e^{-\frac{\tau}{\tau_{trip}}}\right) \frac{1}{N} \left(\frac{f_1}{1 + \frac{\tau}{\tau_{D1}} \sqrt{1 + R^2 \frac{\tau}{\tau_{D1}}}} + \frac{f_2}{1 + \frac{\tau}{\tau_{D2}} \sqrt{1 + R^2 \frac{\tau}{\tau_{D2}}}} \right)$$

Equation 2

f_1 and f_2 are respectively the fraction of the particles corresponding to faster-diffusing component 1 (dye or free enzyme) or the slower 2 (free enzyme in vesicles), τ_{D1} represents the diffusion time of the dye and τ_{D2} the diffusion time of the vesicles, T the fraction of fluorophores in triplet state with triplet time τ_{trip}, N is the number of particles and R the structural parameter, fixed at 5, according to the guidelines from Zeiss. The τ_{trip} and τ_D of free dye were determined independently, and subsequently fixed in the fitting procedure for dye interaction.

The degree of labelling (DOL) was obtained from the ratio of the counts per molecule (CPM)

$$DOL = \frac{CPM_{labelled\ enzyme}}{CPM_{free\ dye}}$$

Equation 3

and, similarly, the number of enzymes per vesicle was calculated as

$$N_{enzymes} = \frac{CPM_{vesicle}}{CPM_{labelled\ enzyme}}$$

Equation 4

To confirm that the increase in enzyme diffusion times originated only from their encapsulation, BODIPY 630/650 was used to label the vesicles' membranes and compare τ_{D2} (vesicles). A fraction of less than 1% of free dye was detected in this case.

The R_h of the vesicles was calculated, assuming a spherical object, deriving the Stokes-Einstein relation to

$$R_h = \frac{4\tau_D k_B T}{6\omega^2 \pi \eta}$$

Equation 5

Where τ_D is the vesicle's diffusion time, k_B is Boltzmann constant, T is the temperature, ω is the confocal radius and η is the solvent's viscosity.

Encapsulation efficiency calculation

For iNOS, the unencapsulated protein was recovered and quantified using the bicinchonic acid assay (BCA) kit from ThermoFisher Scientific, and a BSA calibration curve. As the expected final sGC concentration was below the lower sensitivity limit for BCA (5 μg mL^{-1}), unencapsulated DyLight 633-labelled sGC was recovered and its absorbance at both 280 and 627 nm was measured with Nanodrop 200 UV-Vis spectrophotometer (ThermoFisher Scientific).

The DOL was calculated using the equation:

$$DOL = \frac{A_{max}\, \varepsilon_{prot}}{(A_{280} - A_{max}\, C_{280})\, \varepsilon_{max}}$$

Equation 6

Where A_{max} is the absorbance of the sample at 627 nm, ε_{prot} is the molar extinction coefficient (in $M^{-1}cm^{-1}$) of the pure protein at 280 nm, A_{280} is the absorbance of the sample at 280 nm, C_{280} is the correction factor of the dye's absorbance at 280 nm (specified by the supplier) and ε_{max} is the molar extinction coefficient of the dye at 627 nm.

The protein concentration measured at 280 nm was estimated for a 70 kDA protein (BRENDA) with ε=72000 M^{-1} cm^{-1} (eXPAsY).

The total amount of both unencapsulated iNOS and sGC was calculated based on the volume and subtracted from the amount originally added, yielding the total concentration in CNCs and the encapsulation efficiency.

Enzymatic fluorescence assays

Enzymatic assays were performed using a Spectramax M5e microplate reader (Molecular Devices, USA) in a 96-well, flat bottomed black plate (Thermo Fisher Scientific) for fluorescence. The final volume in each well was of 200 µL in PBS. Both free and encapsulated enzymes were added at the same concentration to compare the influence of encapsulation on their activity (50 µg mL^{-1} for iNOS and 0.05 µg mL^{-1} for sGC). For iNOS activity, 10 µM arginine was used as substrate and 4,5-diaminofluorescein (DAF-2) was used to detect the reaction, as it reacts with NO forming a fluorescent triazole (Ex. 495 Em. 515 nm)[62] and additional NADPH (final 25 µM) was added to the reactions, so that it was always in excess. Background correction was always performed.

For sGC activity assays, the same concentrations of arginine and NADPH were used, with 20 µM of mant-GTP added. Upon its conversion to mant-cGMP, it increases its fluorescence (Ex. 280 Em. 430 nm). [63] When mant-GTP was co-encapsulated, the values were normalized to a vesicle only solution. For long-running measurements (12 hours), a quartz cuvette was instead used, volume 2.5 mL, with the same concentrations as above. The ratio between CNC activity and free enzyme activity was calculated on the fluorescence intensity at the end of the assay. Relative fluorescence units (RFU) is defined as

$$\boldsymbol{RFU = \frac{PF_{RT}}{CF_{RT}}}$$

Equation 7

where PF_{RT} is the product fluorescence intensity in real time and CF_{RT} is the calibration fluorescence intensity in real time, performed by the instrument.

Cell culturing

HeLa cells (epitheloid cervix carcinoma, human; ATCC, CCL-2) were cultured in DMEM with GlutaMAX™-I supplemented with 10% fetal calf serum (FCS), 100 units/mL penicillin and 100 µg/mL Streptomycin. C2C12 cells (muscle myoblasts, mouse, ATCC, CRL-1772) were cultured

in DMEM with GlutaMAX^{TM}-I supplemented with 20% FCS, 100 units/mL penicillin and 100 µg/mL Streptomycin. Cells were maintained at 37 ºC and 5% CO_2.

Live cell imaging of Hela cells

Freshly trypsinized HeLa cells were seeded at a density of 6 x10^4 cells per well in an 8-well glass bottom ibidi plate. After 24 h, the cell supernatant was removed and replaced with 0.1 mM Fluo-4-AM in FluoroBrite DMEM live cell imaging medium supplemented with 10% FCS and 1% Penicillin/Streptomycin. The cells were incubated for 20 min in presence of the calcium sensitive dye, followed by rinsing 3 times and addition of 300 µL live cell imaging medium. The cells were then dosed with 100 µL of either (a) 1 mg mL^{-1} iNOS-CNCs and 1 mg mL^{-1} sGC-CNC in PBS; (b) 1 mg mL^{-1} iNOS-CNC in PBS alone; (c) 1 mg mL^{-1} sGC-CNC in PBS alone; (d) 2 mg mL^{-1} empty polymersomes as an internal control to ensure the polymer does not cause interference; (e) 0.22 mM NO-donor SNAP and 0.2 mM cGMP in PBS as a positive control; (f) PBS only as a negative control.

After dosing, cells were immediately visualized (lag time: 5 minutes, in order to observe the initial peak) by confocal laser scanning microscopy (CLSM) on a LSM 880 confocal laser microscope with a 40x, 1.2 water immersion C-Apochromat objective lens, using ATTO 488 laser and light path parameters. Cells were imaged continuously for 12 hours, in an enclosed incubator at 37 °C and 5% CO_2, with 1 frame/minute capture and constant diffraction-based refocusing. Fluo-4 intensity depends on the intracellular [Ca^{2+}]. The laser intensity was always kept constant, and exposition time was limited to avoid photobleaching. The fluorescence intensity change over time was measured with ZEN software Black Edition (Zeiss, Germany), by randomly selecting 11 oval ROIs within single cells and following them over the course of the experiment, with no post-processing of the fluorescence signal. To control for any residual photobleaching effect, or the

eventual natural excretion of the dye over time, cells loaded with only Fluo-4 AM were used as baseline. To better visualize the differences in fluorescence, ZEN software was used to enhance the resulting color signal in the movies (best fit).

To visualize the CNC uptake and determine the effect of the CNCs after uptake, the procedure described above was slightly modified. Cells were plated at the same seeding density and cultured for 24 h. After 24 h the supernatant was removed and replaced with 300 µL supplemented DMEM and 100 µL of (a) 1 mg mL^{-1} iNOS-ATTO488-labeled CNCs and 1 mg mL^{-1} sGC-DY Light 633-labeled CNCs in PBS; or (b) 1 mg/mL^{-1} iNOS-CNCs and 1 mg mL^{-1} sGC-CNC in PBS. After 24 h incubation, the supernatant was removed. In the case of the fluorescently labelled CNCs, the cells were directly imaged *via* CLSM, 12 hours, 1 frame/minute. In the case of the non-labelled CNCs (sample b above), the supernatant was replaced with the 0.1 mM Fluo-4-AM solution. The cells were incubated for 20 min in presence of Fluo-4-AM, followed by rinsing 3 times and addition of 400 µL live cell imaging medium.

Live cell imaging of C2C12 cells

Freshly trypsinized C2C12 cells were seeded at a density of $3x10^3$ cells per well in an 8-well glass bottom Ibidi plate. After 24 h, the cell supernatant was removed and replaced with differentiating medium (DMEM supplemented with 2% horse serum). The cells were differentiated for 5 days. After 5 days the supernatant was removed and replaced with 0.1 mM Fluo-4-AM in live cell imaging medium as described above. The cells were incubated for 20 min in presence of the calcium sensitive dye, followed by rinsing 3 times and addition of 300 µL live cell imaging medium. The cells were then dossed with 100 µL of either (a) 1 mg mL^{-1} iNOS-CNCs and 1 mg mL^{-1} sGC-CNC in PBS; (b) 0.22 mM NO-donor SNAP and 0.2 mM cGMP in PBS as a

positive control; (c) PBS only as a negative control. After dosing, cells were immediately visualized by CLSM using the same settings described above for the HeLa live cell imaging.

To determine the effect of CNCs after uptake, the procedure described above was slightly modified. C2C12 cells were plated at the same seeding density and differentiated for 5 days as described above. After 5 days the supernatant was removed and replaced with 300 µL supplemented DMEM and 100 µL solution of 1 mg mL^{-1} iNOS-CNCs and 1 mg mL^{-1} sGC-CNC in PBS. After a 24 h incubation, the supernatant was replaced with the 0.1 mM Fluo-4-AM solution. The cells were incubated for 20 min in presence of Fluo-4-AM, followed by rinsing 3 times and addition of 400 µL live cell imaging medium.

ASSOCIATED CONTENT

The following files are available free of charge and are available online on the ACS Publications website.

Supporting Information (PDF). Fig. S1: concentration of vesicles measured by NTA. Fig. S2: FCS curves of labelled enzymes and vesicles. Fig. S3: cascade of free enzymes, controls of iNOS- and sGC-CNC in a cascade. Fig. S4: further controls with free and vesicle-adsorbed enzymes. Fig. S5: the complex kinetics of CNCs at higher substrate or enzymes concentrations. Fig. S6: z-stack orthogonal views of internalized CNCs. Fig. S7: normalized fluorescence profiles of HeLa cells. Movie S1 (AVI): unspecific uptake of fluorescent CNC. Movie S2 (AVI): live imaging of HeLa cells with Fluo-4 and external CNCs. Movie S3 (AVI): live imaging of C2C12 with internalized CNCs.

AUTHOR INFORMATION

Corresponding Author

* Department of Chemistry, University of Basel, Mattenstrasse 24a, BPR 1096, 4058 Basel, Switzerland

Author Contributions

The manuscript was written through contributions of all authors. All authors have given approval to the final version of the manuscript.

ACKNOWLEDGMENT

We gratefully acknowledge the financial support provided by the Swiss National Science Foundation, the National Centre of Competence in Research - Molecular Systems Engineering, and the University of Basel. The authors thank Dr. Mariana Spulber for the concept and the preliminary exploration of the cascade reaction in CNCs. Additionally, the authors thank Prof. Wolfgang P. Meier (Chemistry Department, University of Basel) for providing the polymer and Dr. Adrian I. Dinu for its synthesis, Dr. Tomaž Einfalt (Pharmazentrum, University of Basel) for useful discussions and suggestions on FCS measurements and Felix Erb for help with optimization of the enzymatic assays.

REFERENCES

1. Ruiz-Stewart, I.; Tiyyagura, S. R.; Lin, J. E.; Kazerounian, S.; Pitari, G. M.; Schulz, S.; Martin, E.; Murad, F.; Waldman, S. A., Guanylyl Cyclase Is An Atp Sensor Coupling Nitric Oxide Signaling To Cell Metabolism. *Proc. Natl. Acad. Sci. U. S. A.* **2004,** *101*, 37-42.
2. Jennissen, K.; Haas, B.; Kunz, W. S.; Pfeifer, A., Cgmp And Camp Differentially Regulate Differentiation And Function Of Brown Adipocytes. *BMC Pharmacol.* **2011,** *11*, P37-P37.
3. Ischiropoulos, H., Protein Modifications By Nitric Oxide And Reactive Nitrogen Species. In *Cell Signaling In Vascular Inflammation*, Bhattacharya, J., Ed. Humana Press: Totowa, 2005; Pp 23-26.

4. Albina, J. E.; Reichner, J. S., Role Of Nitric Oxide In Mediation Of Macrophage Cytotoxicity And Apoptosis. *Cancer Metastasis Rev.* **1998,** *17*, 39-53.
5. Chanthaphavong, R. S.; Loughran, P. A.; Lee, T. Y.; Scott, M. J.; Billiar, T. R., A Role For Cgmp In Inducible Nitric-Oxide Synthase (Inos)-Induced Tumor Necrosis Factor (Tnf) Alpha-Converting Enzyme (Tace/Adam17) Activation, Translocation, And Tnf Receptor 1 (Tnfr1) Shedding In Hepatocytes. *J. Biol. Chem.* **2012,** *287*, 35887-98.
6. Gnipp, S.; Mergia, E.; Puschkarow, M.; Bufe, A.; Koesling, D.; Peters, M., Nitric Oxide Dependent Signaling Via Cyclic Gmp In Dendritic Cells Regulates Migration And T-Cell Polarization. *Sci. Rep.* **2018,** *8*, 10969.
7. Zamora, R.; Vodovotz, Y.; Billiar, T. R., Inducible Nitric Oxide Synthase And Inflammatory Diseases. *Molecular Medicine (Cambridge, Mass.)* **2000,** *6*, 347-373.
8. Tidball, J. G.; Wehling-Henricks, M., Nitric Oxide Synthase Deficiency And The Pathophysiology Of Muscular Dystrophy. *The Journal Of Physiology* **2014,** *592*, 4627-4638.
9. Zhao, H. J.; Wang, S.; Cheng, H.; Zhang, M.-Z.; Takahashi, T.; Fogo, A. B.; Breyer, M. D.; Harris, R. C., Endothelial Nitric Oxide Synthase Deficiency Produces Accelerated Nephropathy In Diabetic Mice. *J. Am. Soc. Nephrol.* **2006,** *17*, 2664.
10. Lind, M.; Hayes, A.; Caprnda, M.; Petrovic, D.; Rodrigo, L.; Kruzliak, P.; Zulli, A., Inducible Nitric Oxide Synthase: Good Or Bad? *Biomed. Pharmacother.* **2017,** *93*, 370-375.
11. Lucas, K. A.; Pitari, G. M.; Kazerounian, S.; Ruiz-Stewart, I.; Park, J.; Schulz, S.; Chepenik, K. P.; Waldman, S. A., Guanylyl Cyclases And Signaling By Cyclic Gmp. *Pharmacol. Rev.* **2000,** *52*, 375-414.
12. Durham, J. P., Guanylate Cyclase: Assay And Properties Of The Particulate And Supernatant Enzymes In Mouse Parotid. *Eur. J. Biochem.* **1976,** *61*, 535-44.
13. Baehr, W.; Karan, S.; Maeda, T.; Luo, D. G.; Li, S.; Bronson, J. D.; Watt, C. B.; Yau, K. W.; Frederick, J. M.; Palczewski, K., The Function Of Guanylate Cyclase 1 And Guanylate Cyclase 2 In Rod And Cone Photoreceptors. *J. Biol. Chem.* **2007,** *282*, 8837-47.
14. Alberts B, J. A., Lewis J., The Compartmentalization Of Cells. In *Mol. Biol. Cell*, 4th Ed.; Garland Science: New York, 2002.
15. Zecchin, A.; Stapor, P. C.; Goveia, J.; Carmeliet, P., Metabolic Pathway Compartmentalization: An Underappreciated Opportunity? *Curr. Opin. Biotechnol.* **2015,** *34*, 73-81.
16. Kuchler, A.; Yoshimoto, M.; Luginbuhl, S.; Mavelli, F.; Walde, P., Enzymatic Reactions In Confined Environments. *Nat Nanotechnol* **2016,** *11*, 409-20.
17. Sakr, O. S.; Borchard, G., Encapsulation Of Enzymes In Layer-By-Layer (Lbl) Structures: Latest Advances And Applications. *Biomacromolecules* **2013,** *14*, 2117-2135.
18. Tanner, P.; Onaca, O.; Balasubramanian, V.; Meier, W.; Palivan, C. G., Enzymatic Cascade Reactions Inside Polymeric Nanocontainers: A Means To Combat Oxidative Stress. *Chemistry (Easton)* **2011,** *17*, 4552-60.
19. Belluati, A.; Craciun, I.; Meyer, C. E.; Rigo, S.; Palivan, C. G., Enzymatic Reactions In Polymeric Compartments: Nanotechnology Meets Nature. *Curr. Opin. Biotechnol.* **2019,** *60*, 53-62.
20. Liu, J.; Postupalenko, V.; Lörcher, S.; Wu, D.; Chami, M.; Meier, W.; Palivan, C. G., DNA-Mediated Self-Organization Of Polymeric Nanocompartments Leads To Interconnected Artificial Organelles. *Nano Lett.* **2016,** *16*, 7128-7136.

21. Marguet, M.; Bonduelle, C.; Lecommandoux, S., Multicompartmentalized Polymeric Systems: Towards Biomimetic Cellular Structure And Function. *Chem. Soc. Rev.* **2013,** *42*, 512-29.
22. Schoonen, L.; Van Hest, J. C. M., Compartmentalization Approaches In Soft Matter Science: From Nanoreactor Development To Organelle Mimics. *Adv. Mater.* **2016,** *28*, 1109-1128.
23. Belluati, A.; Thamboo, S.; Najer, A.; Maffeis, V.; Von Planta, C.; Craciun, I.; Palivan, C. G.; Meier, W., Multicompartment Polymer Vesicles With Artificial Organelles For Signal-Triggered Cascade Reactions Including Cytoskeleton Formation. *Adv. Funct. Mater. N/A*, 2002949.
24. Van Oppen, L. M. P. E.; Abdelmohsen, L. K. E. A.; Van Emst-De Vries, S. E.; Welzen, P. L. W.; Wilson, D. A.; Smeitink, J. A. M.; Koopman, W. J. H.; Brock, R.; Willems, P. H. G. M.; Williams, D. S.; Van Hest, J. C. M., Biodegradable Synthetic Organelles Demonstrate Ros Shielding In Human-Complex-I-Deficient Fibroblasts. *ACS Central Science* **2018,** *4*, 917-928.
25. Nishimura, T.; Akiyoshi, K., Biotransporting Biocatalytic Reactors Toward Therapeutic Nanofactories. *Adv Sci (Weinh)* **2018,** *5*, 1800801.
26. Belluati, A.; Craciun, I.; Liu, J.; Palivan, C. G., Nanoscale Enzymatic Compartments In Tandem Support Cascade Reactions *In Vitro*. *Biomacromolecules* **2018,** *19*, 4023-4033.
27. Tanner, P.; Balasubramanian, V.; Palivan, C. G., Aiding Nature's Organelles: Artificial Peroxisomes Play Their Role. *Nano Lett.* **2013,** *13*, 2875-2883.
28. Aliancy, J.; Stamer, W. D.; Wirostko, B., A Review Of Nitric Oxide For The Treatment Of Glaucomatous Disease. *Ophthalmol. Ther.* **2017,** *6*, 221-232.
29. Chandrawati, R.; Chang, J. Y. H.; Reina-Torres, E.; Jumeaux, C.; Sherwood, J. M.; Stamer, W. D.; Zelikin, A. N.; Overby, D. R.; Stevens, M. M., Localized And Controlled Delivery Of Nitric Oxide To The Conventional Outflow Pathway Via Enzyme Biocatalysis: Toward Therapy For Glaucoma. *Adv. Mater.* **2017,** *29*, 1604932.
30. Greene Stephen, J.; Gheorghiade, M.; Borlaug Barry, A.; Pieske, B.; Vaduganathan, M.; Burnett John, C.; Roessig, L.; Stasch, J. P.; Solomon Scott, D.; Paulus Walter, J.; Butler, J., The Cgmp Signaling Pathway As A Therapeutic Target In Heart Failure With Preserved Ejection Fraction. *J. Am. Heart Assoc.*, E000536.
31. Mackenzie, A.; Wadsworth, R. M., Extracellular L-Arginine Is Required For Optimal No Synthesis By Enos And Inos In The Rat Mesenteric Artery Wall. *Br. J. Pharmacol.* **2003,** *139*, 1487-1497.
32. Mancinelli, R.; La Rovere, R. M. L.; Fulle, S.; Miscia, S.; Marchisio, M.; Pierdomenico, L.; Lanuti, P.; Procino, G.; Barbieri, C.; Svelto, M.; Fanò-Illic, G.; Pietrangelo, T., Extracellular Gtp Is A Potent Water-Transport Regulator Via Aquaporin 5 Plasma-Membrane Insertion In M1-Ccd Epithelial Cortical Collecting Duct Cells. *Cell. Physiol. Biochem.* **2014,** *33*, 731-746.
33. Pietrangelo, T.; Fioretti, B.; Mancinelli, R.; Catacuzzeno, L.; Franciolini, F.; Fanò, G.; Fulle, S., Extracellular Guanosine-5'-Triphosphate Modulates Myogenesis Via Intermediate Ca(2+)-Activated K+ Currents In C2c12 Mouse Cells. *J. Physiol.* **2006,** *572*, 721-733.
34. Lomora, M.; Itel, F.; Dinu, I. A.; Palivan, C. G., Selective Ion-Permeable Membranes By Insertion Of Biopores Into Polymersomes. *PCCP* **2015,** *17*, 15538-15546.
35. Belluati, A.; Mikhalevich, V.; Yorulmaz Avsar, S.; Daubian, D.; Craciun, I.; Chami, M.; Meier, W. P.; Palivan, C. G., How Do The Properties Of Amphiphilic Polymer Membranes Influence The Functional Insertion Of Peptide Pores? *Biomacromolecules* **2019**.

36. Stauch, O.; Schubert, R.; Savin, G.; Burchard, W., Structure Of Artificial Cytoskeleton Containing Liposomes In Aqueous Solution Studied By Static And Dynamic Light Scattering. *Biomacromolecules* **2002,** *3*, 565-78.
37. Garni, M.; Einfalt, T.; Goers, R.; Palivan, C. G.; Meier, W., Live Follow-Up Of Enzymatic Reactions Inside The Cavities Of Synthetic Giant Unilamellar Vesicles Equipped With Membrane Proteins Mimicking Cell Architecture. *ACS Synth. Biol.* **2018,** *7*, 2116-2125.
38. Ferguson, J. W.; Dover, A. R.; Chia, S.; Cruden, N. L.; Hayes, P. C.; Newby, D. E., Inducible Nitric Oxide Synthase Activity Contributes To The Regulation Of Peripheral Vascular Tone In Patients With Cirrhosis And Ascites. *Gut* **2006,** *55*, 542-6.
39. Zhao, Y.; Brandish, P. E.; Ballou, D. P.; Marletta, M. A., A Molecular Basis For Nitric Oxide Sensing By Soluble Guanylate Cyclase. *Proc. Natl. Acad. Sci. U. S. A.* **1999,** *96*, 14753.
40. Wang, J.; Bafna, J. A.; Bhamidimarri, S. P.; Winterhalter, M., Small-Molecule Permeation Across Membrane Channels: Chemical Modification To Quantify Transport Across Ompf. *Angew. Chem. Int. Ed.* **2019,** *58*, 4737-4741.
41. Rostovtseva, T. K.; Nestorovich, E. M.; Bezrukov, S. M., Partitioning Of Differently Sized Poly(Ethylene Glycol)S Into Ompf Porin. *Biophys. J.* **2002,** *82*, 160-169.
42. Tsai, A. L.; Berka, V.; Sharina, I.; Martin, E., Dynamic Ligand Exchange In Soluble Guanylyl Cyclase (Sgc): Implications For Sgc Regulation And Desensitization. *J. Biol. Chem.* **2011,** *286*, 43182-92.
43. Ballou, D. P.; Zhao, Y.; Brandish, P. E.; Marletta, M. A., Revisiting The Kinetics Of Nitric Oxide (No) Binding To Soluble Guanylate Cyclase: The Simple No-Binding Model Is Incorrect. *Proc. Natl. Acad. Sci. U. S. A.* **2002,** *99*, 12097-12101.
44. Lee, Y. C.; Martin, E.; Murad, F., Human Recombinant Soluble Guanylyl Cyclase: Expression, Purification, And Regulation. *Proc. Natl. Acad. Sci. U. S. A.* **2000,** *97*, 10763-8.
45. Lomora, M.; Gunkel-Grabole, G.; Mantri, S.; Palivan, C. G., Bio-Catalytic Nanocompartments For *In Situ* Production Of Glucose-6-Phosphate. *Chem. Commun.* **2017,** *53*, 10148-10151.
46. Einfalt, T.; Witzigmann, D.; Edlinger, C.; Sieber, S.; Goers, R.; Najer, A.; Spulber, M.; Onaca-Fischer, O.; Huwyler, J.; Palivan, C. G., Biomimetic Artificial Organelles With *In Vitro* And *In Vivo* Activity Triggered By Reduction In Microenvironment. *Nat. Comm.* **2018,** *9*, 1127.
47. Wright, G.; Srinivasan, K.; Janetopoulos, C., Phagocytosis. In *Encyclopedia Of Biological Chemistry (Second Edition)*, Lennarz, W. J.; Lane, M. D., Eds. Academic Press: Waltham, 2013; Pp 437-440.
48. Au - Lee, W.-K.; Au - Dittmar, T., Cytosolic Calcium Measurements In Renal Epithelial Cells By Flow Cytometry. *Jove* **2014**, E51857.
49. Francis, S. H.; Busch, J. L.; Corbin, J. D.; Sibley, D., Cgmp-Dependent Protein Kinases And Cgmp Phosphodiesterases In Nitric Oxide And Cgmp Action. *Pharmacol. Rev.* **2010,** *62*, 525-563.
50. Cabrera-Pastor, A.; Taoro-González, L.; Cuñat, A. N.; Canet-López, D.; Balzano, T.; Felipo, V., Extracellular Cyclic Gmp Modulates Membrane Expression Of The Glua1 And Glua2 Subunits Of Ampa Receptor In Cerebellum: Molecular Mechanisms Involved. *Sci. Rep.* **2017,** *7*, 17656.
51. Hirsch, J. R.; Weber, G.; Kleta, I.; Schlatter, E., Cgmp Serves As An Extracellular Regulator Of A Ca2+-Dependent K+ Channel In Immortalized Human Proximal Tubule Cells. *Cell. Physiol. Biochem.* **2001,** *11*, 77-82.

52. Hou, Y.; Lascola, J.; Dulin, N. O.; Ye, R. D.; Browning, D. D., Activation Of Cgmp-Dependent Protein Kinase By Protein Kinase C. *J. Biol. Chem.* **2003,** *278*, 16706-16712.
53. Abdel-Latif, A. A., Cross Talk Between Cyclic Nucleotides And Polyphosphoinositide Hydrolysis, Protein Kinases, And Contraction In Smooth Muscle. *Exp. Biol. Med.* **2001,** *226*, 153-163.
54. Mcmahon, D. K.; Anderson, P. A.; Nassar, R.; Bunting, J. B.; Saba, Z.; Oakeley, A. E.; Malouf, N. N., C2c12 Cells: Biophysical, Biochemical, And Immunocytochemical Properties. *Am. J. Physiol. Cell Physiol.* **1994,** *266*, C1795-C1802.
55. Kakizawa, S.; Yamazawa, T.; Iino, M., Nitric Oxide-Induced Calcium Release: Activation Of Type 1 Ryanodine Receptor By Endogenous Nitric Oxide. *Channels (Austin, Tex.)* **2013,** *7*, 1-5.
56. Charles, A., Nitric Oxide Pumps Up Calcium Signalling. *Nat. Cell Biol.* **1999,** *1*, E193-E195.
57. Gross, S. M.; Rotwein, P., Live Cell Imaging Reveals Marked Variability In Myoblast Proliferation And Fate. *Skeletal Muscle* **2013,** *3*, 10.
58. Botta, A.; Malena, A.; Loro, E.; Del Moro, G.; Suman, M.; Pantic, B.; Szabadkai, G.; Vergani, L., Altered Ca2+ Homeostasis And Endoplasmic Reticulum Stress In Myotonic Dystrophy Type 1 Muscle Cells. *Genes* **2013,** *4*, 275-292.
59. Pauly, M.; Angebault-Prouteau, C.; Dridi, H.; Notarnicola, C.; Scheuermann, V.; Lacampagne, A.; Matecki, S.; Fauconnier, J., Er Stress Disturbs Sr/Er-Mitochondria Ca2+ Transfer: Implications In Duchenne Muscular Dystrophy. *Biochim. Biophys. Acta - Molecular Basis Of Disease* **2017,** *1863*, 2229-2239.
60. Baumann, P.; Spulber, M.; Dinu, I. A.; Palivan, C. G., Cellular Trojan Horse Based Polymer Nanoreactors With Light-Sensitive Activity. *J. Phys. Chem. B* **2014,** *118*, 9361-9370.
61. Battaglia, G.; Ryan, A. J., Pathways Of Polymeric Vesicle Formation. *J. Phys. Chem. B* **2006,** *110*, 10272-10279.
62. Sutherland, H.; Zolle, O.; Khundkar, R.; Simpson, A. W.; Jarvis, J. C.; Salmons, S., A Nonradioactive Assay For Nitric Oxide Synthase Activity In Tissue Extracts. *Methods Mol. Biol.* **2004,** *279*, 105-11.
63. Newton, M.; Niewczas, I.; Clark, J.; Bellamy, T. C., A Real-Time Fluorescent Assay Of The Purified Nitric Oxide Receptor, Guanylyl Cyclase. *Anal. Biochem.* **2010,** *402*, 129-136.